Thermal conduction through a cool well

Beatrice Baldelli ®,[*] Gaute Linga ®, and Eirik Grude Flekkøy ®
PoreLab, The Njord Centre, Department of Physics, University of Oslo, Oslo 0371, Norway

We study a differentially heated square cavity with inlet and outlet ports at the top of the side walls, quantifying how the effective thermal conductivity changes with the temperature difference across the system. The side walls are insulating, the top surface is kept at a fixed high temperature, and the bottom surface at a fixed low temperature, leading to buoyancy-stabilized flow. We visualize the flow pattern for Reynolds number, Re = 1, and Prandtl number, Pr = 50, and characterize the heat transfer at the bottom surface using the Nusselt number, Nu, for Re = 0.1, 1, 10 and Pr = 1, 50. As the Richardson number, Ri, is increased, we observe the formation of a series of system-spanning vortices through the merging of Moffatt eddies growing from the bottom corners of the cavity. We find that the convection, which enhances the transport of heat, is strongly suppressed by increasing the temperature drop. As a result Nu drops by a factor 1–3 depending on the Reynolds number.

I. INTRODUCTION

Thermal convection has a major impact on the overall transport of thermal energy, as is exemplified by the formation of cumulus clouds or the boiling of a pot of water. These are well-studied processes that are driven by a destabilizing thermal gradient [1]. The opposite case where the thermal gradient is stabilizing and works against convection, is less widely studied. Processes where this happens include the flow of cold water under a warmer surface, as may be the case in geothermal wells [2,3], and lakes [4]. Also, it is well known that surface structure may play a role in the geothermal regulation of certain mammals [5]. Meteorological examples include warm winds over colder valleys. In the present paper, we quantify such heat exchange in the simple case of low Reynolds number flow over a thermally stabilized cavity, where the bottom is maintained at a temperature that is lower than that of the passing fluid. Establishing the effective heat conductivity over a cavity and how it depends on its size and the flow velocity may be applied for the purpose of upscaling in real-world systems where a range of cavity sizes and flow velocities are present.

Flow in a lid-driven cavity in the presence of a temperature gradient has been studied widely [6–10], mostly in the case of a destabilizing thermal gradient. Iwatsu *et al.* [6] study the relative importance of natural and forced convection for several values of the Richardson number in a lid-driven square cavity with insulating side walls and isothermal top and bottom walls, with the top one at a higher temperature than the bottom, i.e., buoyancy stabilized. Cheng and Liu [7] investigate the effect on flow and heat transfer of four temperature gradient directions (upward, downward, leftward, and rightward) in a lid-driven square cavity. They study these four cases for the situation where the lid motion forcing dominates over thermal convection (i.e., low Richardson number, Ri = 0.1), mixed convection (Ri = 1) dominating thermal convection (i.e., high Ri, Ri = 10). They find

---

[*]beatrice.baldelli@fys.uio.no
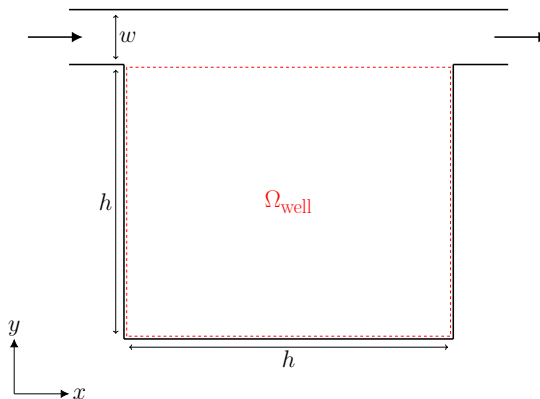
FIG. 1. The system is a square cavity of side h with a narrow channel of width $w = h/60$ at the top. The flow is driven from the left to right in the channel by a constant body force, f.

that both the Richardson number and the temperature affect flow pattern and heat transfer, however, the heat transfer rate increases with decreasing Ri for all four temperature gradient directions.

Several studies [11–14] have also been conducted on flow in a square cavity with inlet and outlet injection ports in the presence of temperature gradients, specifically, on the effect on the flow patterns and heat transfer of the position of the injection ports. Saeidi and Khodadadi [11] visualize flow patterns in a square cavity with fixed inlet port position and nine locations for the outlet port. The walls of the cavity are maintained at a temperature higher than that of the injected fluid. Mahmoudi *et al.* [12] and Koufi *et al.* [13] study the effect of inlet and outlet placement on the flow and temperature field in a square cavity with a warm isothermal bottom wall. Koufi *et al.* [13] study the turbulent flow through a cavity with the other three walls at a fixed cold temperature while Mahmoudi *et al.* [12] have three insulating walls and inject cold fluid.

The system investigated in this study is a square cavity with both inlet and outlet ports at the top of the side walls. The side walls are insulating, while the top and bottom surfaces are isothermal. The study differs from that of the above-mentioned ones [11–13] in that flow is steady and the top surface is at a higher temperature than the bottom one, i.e., the system is buoyancy stabilized, and that we quantify how heat transfer (quantified by the Nusselt number) changes with the temperature difference. In all our simulations the Richardson number is larger than unity, so that forced convection never dominates over thermal convection. The focus of the study is the changes in the qualitative features of the flow patterns and the heat transfer as the Richardson number, Ri, increases. With this goal, we made several series of simulations by fixing the values of the Reynolds and Prandtl numbers, and increasing the values of Ri. In all our simulations the Richardson number is larger than unity, so that forced convection never dominates over thermal convection. We characterize the flow through visualization of the streamlines. The flow patterns in a square lid-driven cavity with a stabilizing thermal gradient orientation have already been studied [6,7]. The flow patterns observed in this case are quite similar to the ones we observe for high values of the Richardson number, Ri, but differ for low Ri due to the presence of open streamlines from the channel. Additionally, we quantify heat transfer through the bottom surface through the Nusselt number, Nu, for several values of Re, Pr, and Ri.

II. SYSTEM DESCRIPTION

A. Geometry

The system shown in Fig. 1 is a two-dimensional square well of height h with a horizontal channel of width $w = h/60$ at the top. A constant force drives flow through the channel, which in turn drives

the flow in the body of the cavity. On the top surface of the well, the temperature is maintained at a constant value, T_+, and on the bottom surface, the temperature is maintained at a lower constant value, T_-. The sides of the cavity are insulating.

B. Governing equations

Since we are interested in the steady state of $\text{Re} \leqslant 10$ flows [15], the equations governing the flow field are the time-independent Navier-Stokes equations,

$$\rho \boldsymbol{u} \cdot \nabla \boldsymbol{u} + \nabla p - \mu \nabla^2 \boldsymbol{u} - f \hat{\boldsymbol{e}}_x - \Delta \rho g \hat{\boldsymbol{e}}_y = \boldsymbol{0}, \tag{1}$$

$$\nabla \cdot \boldsymbol{u} = 0, \tag{2}$$

and the time-independent advection-diffusion equation for the temperature,

$$k \nabla^2 T + \boldsymbol{u} \cdot \nabla T = 0. \tag{3}$$

Here, $\boldsymbol{u}$ is the fluid velocity, p is the pressure, μ is the dynamic viscosity, f is the constant driving force, $\hat{\boldsymbol{e}}_x$ is the unit vector parallel to the channel axis directed from left to right, ρ is the density, β is the thermal compressibility, $\boldsymbol{g}$ is the acceleration of gravity, $\hat{\boldsymbol{e}}_y$ is the unit vector parallel to the side walls pointing to the top surface, k is the heat diffusivity, and T is the temperature.

We adopt the Boussinesq approximation, taking the density to be constant in the inertial term, while the gravitational forcing term in Eq. (1) is given by

$$\Delta \rho \boldsymbol{g} = \rho_0 \beta (T - T_0) \boldsymbol{g}, \tag{4}$$

where $\rho_0 = \rho(T_0)$, and T_0 is a reference temperature.

Although the equations were solved in their dimensional form, the results are better interpreted in light of the adimensional equations:

$$\boldsymbol{u}' \cdot \nabla \boldsymbol{u}' + \nabla p' - \text{Re}^{-1} \nabla^2 \boldsymbol{u}' - \frac{\text{Ri}}{\text{R}_\text{T}} \hat{\boldsymbol{e}}_x - \text{Ri}\, T' \hat{\boldsymbol{e}}_y = 0 \tag{5}$$

$$\nabla \cdot \boldsymbol{u}' = 0 \tag{6}$$

$$(\text{Re}\, \text{Pr})^{-1} \nabla^2 T' + \boldsymbol{u}' \cdot \nabla T' = \boldsymbol{0}, \tag{7}$$

where $\text{Re} = Uh/\nu$ is the Reynolds number, $\text{Ri} = \beta g h \Delta T / U^2$ is the Richardson number, $\text{R}_\text{T} = \beta g \rho \Delta T / f$ is the ratio between the buoyancy force and the driving force in the channel, $\text{Pr} = \nu/k$ is the Prandtl number, $U = \langle |\boldsymbol{u}| \rangle_{(x,y) \in \Omega_\text{well}}$ is the speed averaged over the volume of the cavity ($\Omega_\text{well} = [0, h] \times [0, h]$), h is the height and width of the cavity, ν is the kinematic viscosity, and $\Delta T = T_+ - T_-$ is the temperature difference between the top and bottom surfaces.

To quantify heat transfer through the bottom surface we consider the heat flux density, defined as

$$\boldsymbol{j} = \boldsymbol{u} T - k \nabla T. \tag{8}$$

Since the top surface has a higher fixed temperature than the bottom surface, the system is stable with respect to buoyancy. If the driving force is set to zero, there is no motion in the system. In this case heat transfer happens purely through diffusion, and is described by Fourier's law,

$$\boldsymbol{j} = -k \frac{\Delta T}{h + w} \hat{\boldsymbol{e}}_y. \tag{9}$$

When the driving force is turned on, convection enters the picture, and the heat transfer cannot be described by the above law. We quantify the departure from the case of pure heat diffusion, by describing the heat transfer through the Nusselt number,

$$\text{Nu} = \frac{\langle j_y \rangle_x (h + w)}{k \Delta T}, \tag{10}$$

where $\langle j_y \rangle_x$ is the y component of the measured heat flux density averaged over the cross section of the well. We measure heat flux density at the bottom of the cavity. The Nusselt number can be interpreted as the ratio between an effective heat diffusivity coefficient k_{eff} and the molecular diffusivity coefficient k, i.e. $Nu = k_{eff}/k$.

C. Computational tools

The flow is simulated using the finite element method implemented in the FEniCS framework [16]. The simulations are run with unstructured triangular mesh generated using Meshpy/triangle [17], with a resolution, res = 64, maximum triangle area, $A_{max} = 0.5(h/\text{res})^2$, and minimum angle, $\theta_{min} = 25°$, to ensure a good-quality mesh. This gives a characteristic mesh size $\sim(h/\text{res})$. The full numerical code can be found at a designated Git repository [18].

III. RESULTS

For low values of Ri, the open streamlines from the channel fan out and occupy almost the entire square cavity, as seen in Fig. 2(a). Only the bottom corners are occupied by vortices. Due to the resolution of the simulation, we only see one vortex in each corner, but there is an infinite cascade of Moffatt eddies in each corner, as is known theoretically [19].

As the value of Ri is increased the outer vortex from each cascade grows until the two touch and merge in a cavity-spanning vortex. This process is shown in Fig. 2. As Ri increases further, the same process is repeated by the second-generation eddies as they emerge from the two corners. These vortices grow even larger as Ri increases, and just like the previous couple of vortices, they touch and merge in a cavity-spanning vortex. This process repeats itself with the following pairs of vortices. In Fig. 3, we can see the formation of the second and third cavity-spanning vortices. More vortices are formed after that, but as the velocity in the cavity decreases with increasing Ri, the velocity in the fourth and, potentially, subsequent vortices is so small that fluctuations due to round-off errors become dominant. Figure 4 shows the values of Ri at which the first four cavity-spanning vortices are formed as well as the Nusselt number, Nu, as a function of Ri when Re = 1 and Pr = 50. In the case of pure diffusion, $k_{eff} = k$, and the Nusselt number is unity, Nu = 1. The value of Nu is highest for smaller values of Ri. This is because most of the cavity is filled by the open streamlines of the channel, and convection has a significant role in the heat transport. As the value of Ri increases the cavity becomes filled by the vortices, and the average speed decreases, so that the fluid in the cavity approaches the stationary state where diffusion becomes the dominant factor in the heat transport. This is shown by Nu approaching 1 as Ri increases. Note that while the topological changes to the streamlines are discontinuous in the sense that two eddies become one, there is no corresponding discontinuity in Nu(Ri), however, a weak inflection point corresponding to the formation of the first cavity-spanning vortex can be observed for Re = 1, Pr = 50 (Fig. 4).

Figure 5(a) compares the series from Fig. 4 to two other series with the same Prandtl number, Pr = 50, but different Reynolds numbers, Re = 0.1 and Re = 10. Here, the Nusselt number is shown as a function of the product of the Richardson and Reynolds numbers, $Ri\,Re = \beta g h^2 \Delta T/(U\nu)$, which represents the ratio between the buoyancy and viscous forces. For the same order of magnitude of $Ri\,Re$, the flow pattern and the qualitative behavior of Nu are similar for the three series of data with different values of Re. All three graphs converge towards Nu = 1 for high values of Ri, but the higher the Reynolds number, the more the effective diffusion coefficient departs from the molecular one for low Ri values. This is because the departure from Fourier's law is caused by convection, which is more significant for larger values of the Reynolds number.

Figure 5(b) shows the same, but for a lower Prandtl number, Pr = 1, corresponding to a larger value of the diffusivity. Hence, the relative significance of diffusion with respect to convection has increased. This can be seen in Fig. 5(b), where the values of Nu for small values of Ri are significantly smaller than their corresponding values for Pr = 50 in Fig. 5(a).

(a) Ri $= 1.1 \times 10^1$

(b) Ri $= 4.6 \times 10^1$

(c) Ri $= 7 \times 10^1$

(d) Ri $= 8.2 \times 10^1$

(e) Ri $= 9.4 \times 10^1$

(f) Ri $= 2.4 \times 10^2$
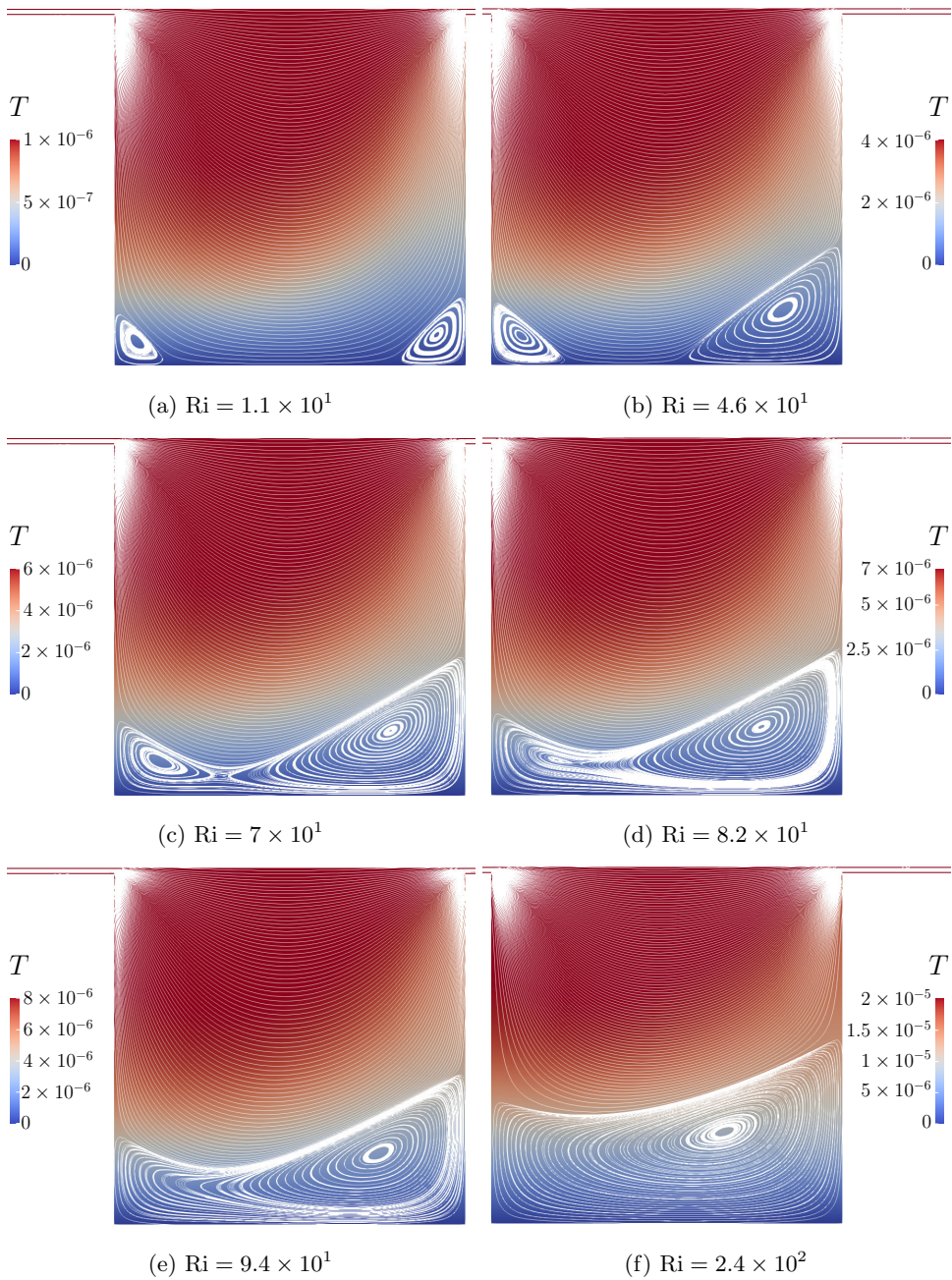
FIG. 2. Temperature field, represented by the color gradient, and streamlines of the velocity field of the steady states for Re $= 1$, Pr $= 50$, and several values of Ri.

IV. CONCLUSIONS

We have studied flow patterns and heat transfer in a square cavity with inlet and outlet ports, insulating side walls, and isothermal high-temperature top wall and low-temperature bottom wall.

(a) Ri $= 1.1 \times 10^3$

(b) Ri $= 1.2 \times 10^3$

(c) Ri $= 2 \times 10^3$

(d) Ri $= 8.5 \times 10^3$
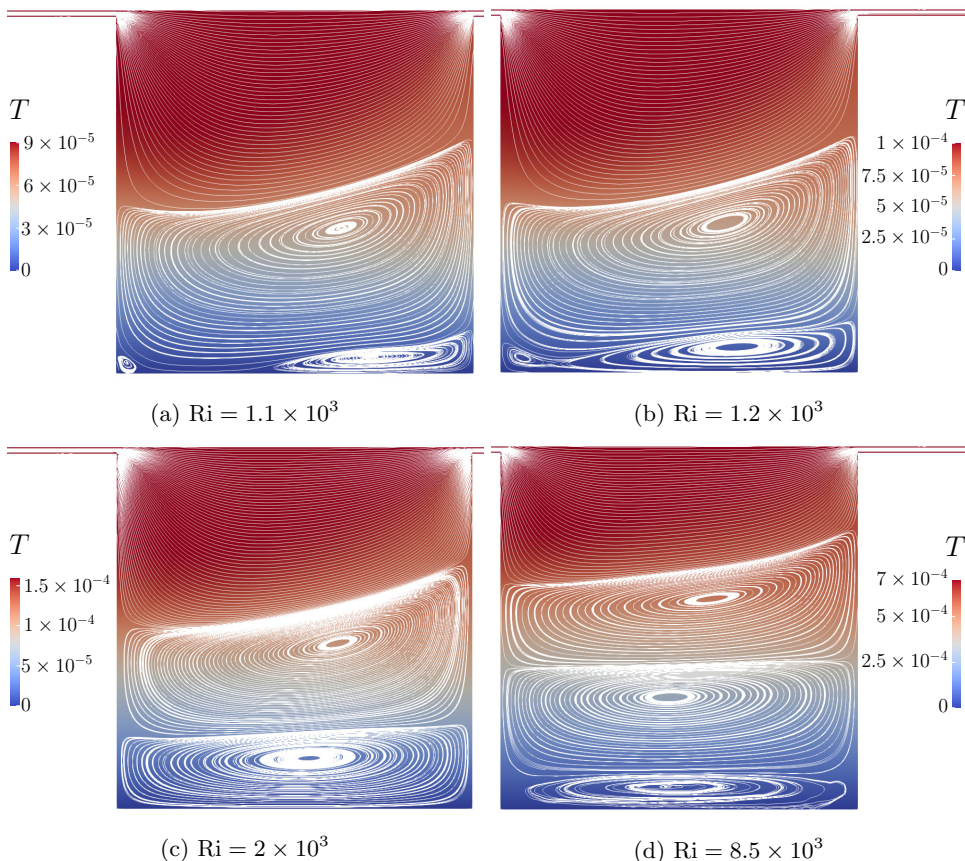
FIG. 3. Temperature field, represented by the color gradient, and streamlines of the velocity field of the steady states for Re $= 1$, Pr $= 50$, and several values of Ri. As Ri increases, more Moffatt eddies grow from the corners, and merge to create other system-width-spanning vortices.

For low values of the Richardson number, Ri, the cavity is filled by open streamlines and the flow is from the inlet to the outlet ports, thus increasing the role of convection compared to the case of larger Ri. As Ri is increased, the outermost Moffatt eddies from the bottom corners expand, merge, and create a series of cavity-spanning vortices.

The heat transfer has been quantified by the Nusselt number, Nu. This is largest for low values of Ri, but converges to unity as Ri increases for all simulation series run, Re $= 0.1, 1, 10$, and Pr $= 1, 50$. Increasing Ri increases the spatial domain of recirculation zones where the main transport mechanism is thermal diffusion. In some cases (Re $= 10$, Pr $= 50$), Nu is decreased by a factor ~ 3 as the temperature difference is increased. Reducing Pr reduces this effect. However, increasing the flow velocity or forcing has the combined effect of reducing Ri and increasing Re, both of which will enhance the heat transport.

An experimental example of the system could be realized by setting the value of the Prandtl number to Pr $= 7$, which is the value for water at the temperature $T = 20\,^\circ$C. Choosing the dimensions of the cavity to be $h = 0.1$ m and $w = 1.67 \times 10^{-3}$ m, the bottom surface temperature to be $T_- = 20\,^\circ$C, and the velocity in the channel to be $u_{\mathrm{ch}} = 2.81 \times 10^{-3}$ ms^{-1}, leads to the value of Reynolds number in the cavity of Re $= 10$. Our simulations predict that, as the temperature difference $\Delta T = T_+ - T_-$ drops from $\Delta T = 6\,^\circ$C to $\Delta T = 6 \times 10^{-5}\,^\circ$C, the Nusselt number, Nu,
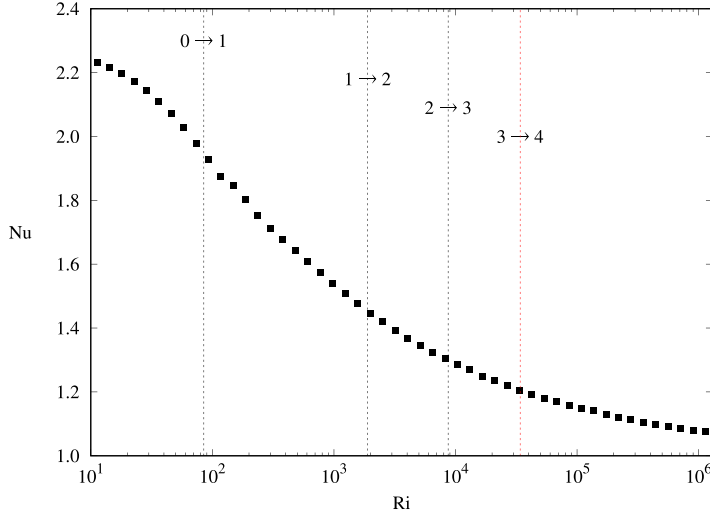
FIG. 4. Nusselt number, Nu, as a function of the Richardson number, Ri, for Reynolds number, Re = 1, and Prandtl number, Pr = 50. The vertical lines indicate the value of Ri at which width-spanning vortices are formed. The labels $n \to n+1$ specify that the formation of a width-spanning vortex has increased the number of vortices from n to $n+1$. After the third vortex, observing new formations becomes difficult because the velocities in the new vortices are so small that they are not properly resolved by the software.

doubles in value: $\text{Nu}(\Delta T = 6\,°\text{C}) = 1.08$, $\text{Nu}(\Delta T = 6 \times 10^{-5}\,°\text{C}) = 2.14$. At given values of Ri and Re, which are computed for the flow inside the cavity, we expect the above numbers to change only weakly if the channel width is changed.

The increase of Nu with decreasing Ri Re is more pronounced for higher values of Re and Pr. We cannot arbitrarily increase Re, since the turbulent regime cannot be reached by the simulations. What can be increased is Pr, which depends on material characteristics and temperature. The example proposed above is for water at $T = 20\,°\text{C}$, which has $\text{Pr} \approx 7$. The Prandtl number of water increases
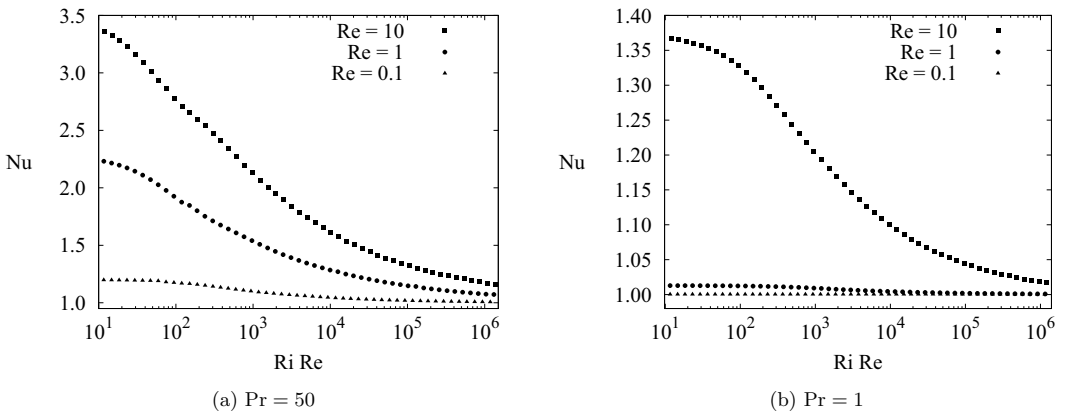
(a) Pr = 50

(b) Pr = 1

FIG. 5. Nusselt number, Nu, as a function of the product of the Richardson and Reynolds numbers Ri Re, for Prandtl number, (a) Pr = 50, (b) Pr = 1 and several values of the Reynolds number, Re. The product Ri Re is proportional to the temperature difference, $\text{Ri Re} = \gamma \Delta T$, however the proportionality constant, γ changes for different values of the Prandtl and Reynolds number: $\gamma(\text{Pr} = 50; \text{Re} = 10) = 10^6$, $\gamma(\text{Pr} = 50; \text{Re} = 1) = 10^7$, $\gamma(\text{Pr} = 50; \text{Re} = 0.1) = 10^8$, $\gamma(\text{Pr} = 1; \text{Re} = 10, 1, 0.1) = 10^8$.

as the temperature decreases. For example, water at $T = 0\,^{\circ}\text{C}$ has $\text{Pr} \approx 14$. There are other fluids with much larger values of Pr; oils have $\text{Pr} = 50 - 10^5$, and glycerin at $T = 25\,^{\circ}\text{C}$ has $\text{Pr} \approx 7 \times 10^3$. Running simulations for $\text{Pr} = 7 \times 10^3$, $\text{Re} = 0.1$, and $10 < \text{Ri Re} < 10^6$, we found that the Nusselt number decreases from $\text{Nu} = 5$ to $\text{Nu} = 1$. Further study is needed for higher values of the Prandtl number.

ACKNOWLEDGMENTS

[1] S. Chandrasekhar, *Hydrodynamic and Hydromagnetic Stability* (Dover Publications, 2013).

[2] A. Neuville, R. Toussaint, and J. Schmittbuhl, Hydrothermal coupling in a self-affine rough fracture, Phys. Rev. E **82**, 036317 (2010).

[3] A. Neuville, E. G. Flekkøy, and R. Toussaint, Influence of asperities on fluid and thermal flow in a fracture: A coupled lattice Boltzmann study, J. Geophys. Res.: Solid Earth **118**, 3394 (2013).

[4] R. Schwefel, A. Gaudard, A. Wüest, and D. Bouffard, Effects of climate change on deepwater oxygen and winter mixing in a deep lake (Lake Geneva): Comparing observational findings and modeling, Water Resour. Res. **52**, 8811 (2016).

[5] C. L. Myhrvold, H. A. Stone, and E. Bou-Zeid, What is the use of elephant hair? PLoS One **7**, e47018 (2012).

[6] R. Iwatsu, J. M. Hyun, and K. Kuwahara, Mixed convection in a driven cavity with a stable vertical temperature gradient, Int. J. Heat Mass Transf. **36**, 1601 (1993).

[7] T. Cheng and W.-H. Liu, Effect of temperature gradient orientation on the characteristics of mixed convection flow in a lid-driven square cavity, Comput. Fluids **39**, 965 (2010).

[8] X. Wen, L.-P. Wang, and Z. Guo, Development of unsteady natural convection in a square cavity under large temperature difference, Phys. Fluids **33**, 084108 (2021).

[9] A. K. Prasad and J. R. Koseff, Combined forced and natural convection heat transfer in a deep lid-driven cavity flow, Int. J. Heat Fluid Flow **17**, 460 (1996).

[10] S. Roy and T. Basak, Finite element analysis of natural convection flows in a square cavity with non-uniformly heated wall(s), Int. J. Eng. Sci. **43**, 668 (2005).

[11] S. Saeidi and J. Khodadadi, Forced convection in a square cavity with inlet and outlet ports, Int. J. Heat Mass Transf. **49**, 1896 (2006).

[12] A. H. Mahmoudi, M. Shahi, and F. Talebi, Effect of inlet and outlet location on the mixed convective cooling inside the ventilated cavity subjected to an external nanofluid, Int. Commun. Heat Mass Transfer **37**, 1158 (2010).

[13] L. Koufi, Z. Younsi, Y. Cherif, and H. Naji, Numerical investigation of turbulent mixed convection in an open cavity: Effect of inlet and outlet openings, Int. J. Therm. Sci. **116**, 103 (2017).

[14] S. Singh and M. A. R. Sharif, Mixed convective cooling of a rectangular cavity with inlet and exit openings on differentially heated side walls, Numer. Heat Transfer, Part A: Appl. **44**, 233 (2003).

[15] G. K. Batchelor, *An Introduction to Fluid Dynamics*, 1st ed. (Cambridge University Press, Cambridge, 2000).

[16] A. Logg, K.-A. Mardal, and G. Wells, *Automated solution of differential equations by the finite element method: The FEniCS book*, Vol. 84 (Springer Science & Business Media, Berlin, 2012).

[17] Triangle/TetGen interface - MeshPy 2020.1 documentation, 2022.

[18] https://github.com/gautelinga/coolwell/releases/tag/v1.0.0.

[19] H. K. Moffatt, Viscous and resistive eddies near a sharp corner, J. Fluid Mech. **18**, 1 (1964).